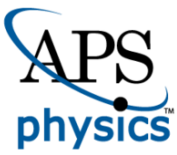

Optical Control of a Single Nuclear Spin in the Solid State

M. L. Goldman, T. L. Patti, D. Levonian, S. F. Yelin, and M. D. Lukin

Phys. Rev. Lett. **124**, 153203 — Published 15 April 2020

DOI: 10.1103/PhysRevLett.124.153203

Optical Control of a Single Nuclear Spin in the Solid State

M. L. Goldman,[1,*] T. L. Patti,[1] D. Levonian,[1] S. F. Yelin,[1,2] and M. D. Lukin[1]

[1] *Department of Physics, Harvard University, Cambridge, Massachusetts 02138, USA*
[2] *Department of Physics, University of Connecticut, Storrs, Connecticut 06269, USA*

We demonstrate a novel method for coherent optical manipulation of individual nuclear spins in the solid state, mediated by the electronic states of a proximal quantum emitter. Specifically, using the nitrogen-vacancy (NV) color center in diamond, we demonstrate control of a proximal ^{14}N nuclear spin via an all-optical Raman technique. We evaluate the extent to which the intrinsic physical properties of the NV center limit the performance of coherent control, and we find that it is ultimately constrained by the relative rates of transverse hyperfine coupling and radiative decay in the NV center's excited state. Possible extensions and applications to other color centers are discussed.

Individual nuclear spins in solid-state materials feature exceptional isolation from the external environment, making them promising candidates for applications such as long-lived quantum memory. For example, the individual electronic spins associated with a nitrogen-vacancy (NV) center in diamond can couple coherently to both the nitrogen nucleus, which is most commonly the spin-1 ^{14}N isotope, and to individual spin-1/2 ^{13}C nuclei in the diamond lattice. Even at room temperature, nuclear spins coupled to NV centers can be read out in a single shot [1] and can have coherence times longer than one second [2]. These properties have encouraged demonstrations of quantum registers consisting of the NV center's electronic spin and either the nitrogen nuclear spin [3], a single ^{13}C nuclear spin [4], or small networks of ^{13}C nuclear spins [5, 6]. Recently, these techniques have enhanced NV-based magnetometry [7] and enabled active quantum error correction [8–10]. However, the substantial isolation of nuclear spins also complicates the initialization and coherent manipulation of nuclear spin states. In particular, the above applications have generally relied on microwave and radio frequency fields for precise control of the electronic and nuclear spins, resulting in poor spatial resolution.

In this Letter, we demonstrate initialization, coherent manipulation, and readout of a single ^{14}N nuclear spin using purely optical methods. There has been extensive interest in using coherent optical techniques to manipulate the NV center's electronic spin, and to implement this spin control in increasingly sophisticated quantum operations [11–16]. In some cases, these techniques are sensitive to the ^{14}N nuclear spin [17–19]. All-optical approaches to spin manipulation feature a much higher spatial resolution—limited, in principle, by the diffraction-limited spot size of the focused manipulation beam—than the traditional spin manipulation techniques that use microwave or radio-frequency radiation [1, 7, 20]. In particular, this makes optical manipulation ideal for densely spaced arrays of color centers integrated into nanophotonic devices [21]. Because this technique makes use of the relatively strong hyperfine coupling between the nuclear spin and the NV center's electronic spin, it can also enable much faster manipulation than traditional techniques that rely on the small gyromagnetic ratio of the nuclear spin [1, 7, 20, 22].

Specifically, we use an optical Raman technique to flip the ^{14}N nuclear spin from the state with $m_I = +1$ to that with $m_I = 0$. We find that the extent to which this population transfer is due to coherent manipulation rather than incoherent pumping is limited by the strength of this hyperfine coupling relative to the decay rate out of the optically excited states that mediate the Raman transition.

We use optical Raman transitions wherein two ground states are optically coupled to a common excited state. Specifically, we couple the states, labeled $|+1\rangle$ and $|0\rangle$, of the NV center's electronic spin-triplet ground state manifold that have electronic spin projections $m_S = +1$ and 0. If the two optical transitions are driven far from resonance, then the states are coupled with an effective Rabi frequency $\tilde{\Omega} = \Omega_0^* \, \Omega_{+1}/\Delta$, where $\Omega_{0(+1)}$ is the Rabi frequency of the transition from $|0\rangle$ ($|+1\rangle$) and Δ is the transitions' single-photon detuning. We must also consider the nuclear degree of freedom, such that our two ground states $|0, m_I^{(0)}\rangle$ and $|+1, m_I^{(+1)}\rangle$ are product states of specific electronic and nuclear spins. Since the ground state of the NV center is an orbital singlet, the selection rules that determine the specific combinations of nuclear spin projections $m_I^{(0)}$ and $m_I^{(+1)}$ that can be coupled by this Raman technique are determined solely by the electronic and nuclear spin characteristics of the intermediate excited state. In order to couple $|0, m_I^{(0)}\rangle$ to $|+1, m_I^{(+1)}\rangle$, the intermediate state must contain a superposition of the product states $|m_S = 0, m_I = m_I^{(0)}\rangle$ and $|m_S = +1, m_I = m_I^{(+1)}\rangle$ so that the optical transitions, which cannot themselves flip either the electronic or nuclear spin, to both ground states are allowed.

Such a superposition of electronic and nuclear spin states is available as a result of an excited state level anticrossing (ESLAC), which has previously been explored in the contexts of nonresonant optical polarization of nearby nuclear spins [23, 26, 27] and early demonstrations of coherent population trapping of the electronic

spin state [12, 28]. As described in the Supplemental Materials [29], two excited states with primarily $m_S = 0$ and $m_S = +1$ character, which we respectively identify as $|E_y\rangle$ and $|E_1\rangle$, can be brought near degeneracy by the application of a magnetic field along the N-V axis. This degeneracy is lifted by three interactions that couple $|E_y\rangle$ with $|E_1\rangle$ [30]. The first two interactions, electronic spin-spin coupling and Zeeman coupling due to magnetic fields perpendicular to the N-V axis, mix $|E_y\rangle$ and $|E_1\rangle$ irrespective of the nuclear degree of freedom and enable Raman transitions that conserve nuclear spin ($m_I^{(0)} = m_I^{(+1)}$). The third interaction, transverse hyperfine coupling with the ^{14}N nuclear spin (which is much stronger in the excited state than in the ground state [27, 31]), provides an electron-nuclear flip-flop interaction ($\propto S_+I_- + S_-I_+$) and enables Raman transitions that conserve the total spin ($m_I^{(0)} = m_I^{(+1)} - 1$). Therefore, by driving optical transitions to $|E_1\rangle$ or $|E_y\rangle$ and setting the two-photon detuning δ_L between the applied optical fields equal to the frequency difference between two ground states, we can drive specific Raman transitions that conserve either the nuclear spin or the total spin.

To explore the nuclear-specific Raman transitions experimentally, we address a single NV center in the sample described in Ref. [32] (see also Supplemental Materials [29]). By holding the sample at a temperature of approximately 7 K, we observe 16 of the 18 possible optical transitions between $^3A_2$ and ^3E [29], which we individually address using three external-cavity diode lasers at 637 nm that are gated by a combination of acousto-optic and electro-optic modulators. The two transitions that are not observed, from $|0\rangle$ to $|A_1\rangle$ and $|A_2\rangle$, are expected to be weaker because of those states' negligible $m_S = 0$ admixture. We drive a Raman transition from $|0\rangle$ to $|+1\rangle$, as shown in Fig. 1(a), by applying two optical driving fields that are detuned by $\Delta \approx 870$ MHz below the transitions from $|0\rangle$ and $|+1\rangle$ to $|E_1\rangle$. Because these two fields are created by modulating a single laser with an electro-optic modulator, their relative phase is stable and their frequency difference δ_L can be controlled precisely. By sweeping δ_L, we map out the multiple hyperfine transitions between $|0\rangle$ and $|+1\rangle$, which are depicted in Fig. 1(b). We perform this spectroscopy by initializing into the electronic $|0\rangle$ state, applying a Raman pulse to drive a transition from $|0\rangle$ to $|+1\rangle$, and then reading out the population remaining in $|0\rangle$.

The results, shown in Fig. 1(c), indicate that this Raman technique is sensitive to the state of the ^{14}N nuclear spin. We observe the three transitions, marked by blue lines, that represent flipping the electronic spin while preserving the nuclear spin, which are commonly observed using traditional microwave manipulation techniques [29]. Crucially, we also observe two other transitions, marked by green lines, that represent driving the

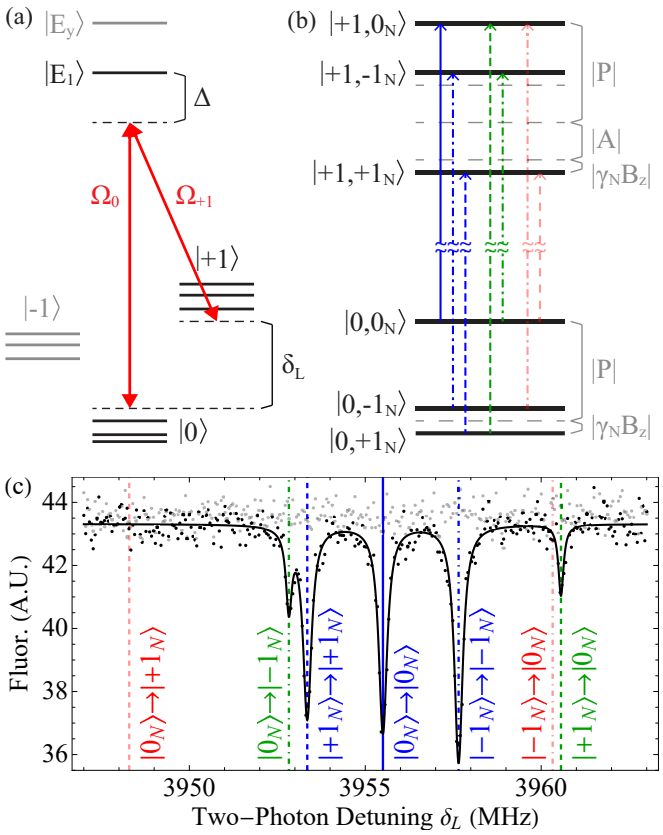

FIG. 1. (a) The Raman transition between the ground states $|0\rangle$ and $|+1\rangle$, which is driven via the optical excited states $|E_1\rangle$ and $|E_y\rangle$. We indicate the two-photon detuning δ_L, the Raman detuning Δ, and the ground state hyperfine structure. (b) The hyperfine structure of the $|0\rangle$ and $|+1\rangle$ electronic states, which depends on the ^{14}N hyperfine coupling A, quadrupolar shift P, and gyromagnetic ratio γ_N. We show the $|0\rangle \rightarrow |+1\rangle$ transitions with $|\Delta m_I| \leq 1$ that conserve the nuclear spin (blue), conserve the total spin (green), and do not conserve spin (red). (c) Spectroscopy of the hyperfine structure of the $|0\rangle \rightarrow |+1\rangle$ Raman transition, with vertical lines marking the fitted energies of the transitions shown in (b). The light grey plot corresponds to a control experiment during which no Raman pulse was applied. The subscript N, here and throughout the Letter, indicates the ^{14}N spin.

electron-nuclear flip-flop transition. We do not observe other transitions, marked by faint red lines, that would conserve neither the total nor the nuclear angular momentum. The relative frequencies of the five observed transitions are determined solely by the ^{14}N axial hyperfine coupling strength A, quadrupole shift P, and axial Zeeman shift $\gamma_N B_z$ [33]. We extract the strength of the nuclear Zeeman shift $\gamma_N B_z/h = -118$ kHz from a measurement of the much larger electronic Zeeman splitting between $|+1\rangle$ and $|-1\rangle$ [29], and the fitted values of $A/h = -2.151(4)$ MHz and $P/h = -4.942(9)$ MHz are in excellent agreement (less than 1% deviation) with pre-

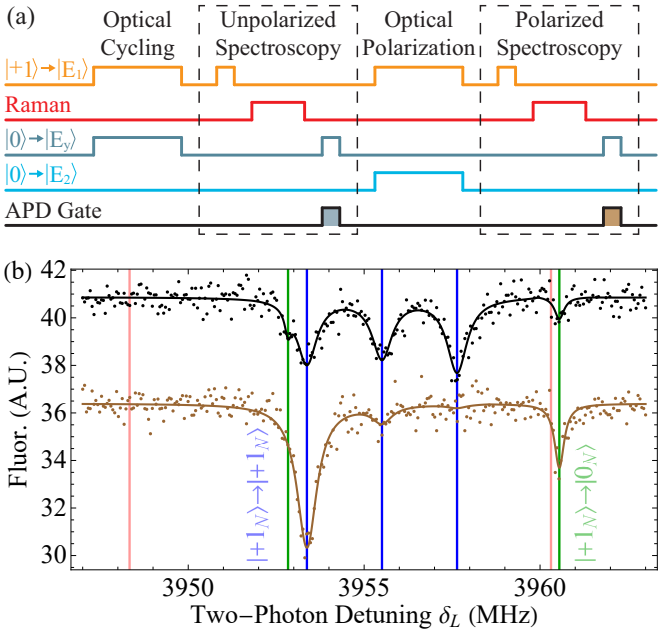

FIG. 2. Optical polarization of the ^{14}N nuclear spin. (a) A schematic diagram of the pulse sequence used to measure the degree of nuclear polarization, which is described in more detail in the Supplemental Materials [29]. (b) Spectroscopy of the $|0\rangle \rightarrow |+1\rangle$ Raman transition, conducted before (black, offset vertically for clarity) and after (brown) 200 μs of optical polarization.

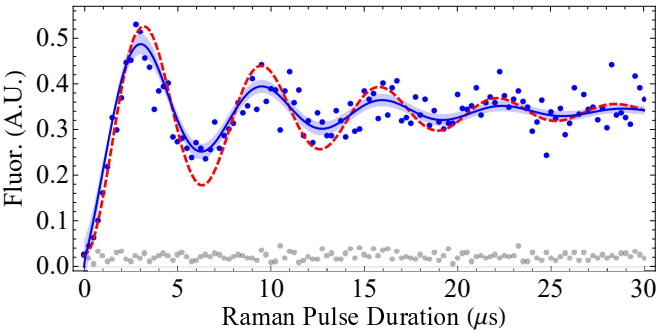

FIG. 3. Nuclear state-selective Raman driving of the electronic spin. After nuclear polarization into $m_I = +1$, a Raman pulse of variable duration is applied on the $|+1_N\rangle \rightarrow |+1_N\rangle$ transition (blue), after which the electronic population in $|+1\rangle$ is measured. The grey data represent a control experiment during which no Raman pulse was applied, the blue plot is a fit to an exponentially damped oscillation with 95% confidence interval, and the red dashed plot is a simulation of the Raman dynamics, as described in the Supplemental Materials [29].

vious measurements [23, 27].

Next, we describe a method for polarizing the ^{14}N nuclear spin via optical pumping. This method relies on simultaneously pumping on the $|+1\rangle \rightarrow |E_1\rangle$ transition and the weakly allowed $|0\rangle \rightarrow |E_2\rangle$ transition, both of which can induce a nuclear spin flip with $\Delta m_I = +1$ when the NV center decays to a different ground state [29]. This method is distinct from the previously observed, nonresonant optical nuclear polarization mechanism [23, 26, 27] in that we can choose, by pumping on the appropriate transitions, to either polarize the nuclear spin or not while optically cycling the electronic spin. We demonstrate this ability in Fig. 2. Using spectroscopy of the hyperfine Raman transitions, we show that the nuclear spin is largely unpolarized after an initial period of optical cycling, which we use to confirm that the NV center is in the correct charge state, and that we can subsequently polarize the nuclear spin by pumping on a different set of optical transitions. The enhancement of the hyperfine transitions originating in $|+1_N\rangle$ and the suppression of all others implies a nuclear polarization of approximately 87 %.

Further, we demonstrate that we can drive coherent oscillations of the electronic spin that are conditioned on the nuclear spin state, as was first observed in Ref. [19]. After initializing the electronic spin to $|0\rangle$ and the nuclear spin to $|+1_N\rangle$, we apply a Raman pulse of variable duration before reading out the population that has been transferred to $|+1\rangle$. As shown in Fig. 3, we observe coherent oscillations of the electronic spin between $|0\rangle$ and $|+1\rangle$ as we vary the length of the Raman pulse.

Finally, we demonstrate coherent manipulation of an electronic-nuclear flip-flop transition. To this end, we first show that we can transfer population from $|+1_N\rangle$ to $|0_N\rangle$ by driving the $|+1_N\rangle \rightarrow |0_N\rangle$ Raman transition. We use a technique that is similar to that used to demonstrate polarization of the nuclear spin in Fig. 2(b) [29]. We polarize the nuclear spin to $|+1_N\rangle$ and the electronic spin to $|0\rangle$ and then either drive the $|+1_N\rangle \rightarrow |0_N\rangle$ transition or wait for an equivalent length of time before performing spectroscopy of the Raman transitions. The results of the spectroscopy, which are shown in Fig. 4(a), indicate that applying the Raman pulse on the $|+1_N\rangle \rightarrow |0_N\rangle$ transition indeed transfers population from $|+1_N\rangle$ to $|0_N\rangle$. Without the $|+1_N\rangle \rightarrow |0_N\rangle$ Raman pulse (black plot), the peaks that correspond to Raman transitions originating in $|+1_N\rangle$ are more prominent, but when the $|+1_N\rangle \rightarrow |0_N\rangle$ Raman pulse is applied (brown plot), the peaks that correspond to Raman transitions originating in $|0_N\rangle$ are more prominent and those that correspond to Raman transitions originating in $|+1_N\rangle$ are suppressed. This indicates that we can transfer nuclear population optically.

To probe the dynamics of nuclear population transfer, we vary the length of the $|+1_N\rangle \rightarrow |0_N\rangle$ Raman pulse and measure the subsequent populations of $|+1_N\rangle$ and $|0_N\rangle$. To read out the nuclear spin state, we map it to the electronic spin state by applying a π pulse on one of the three nuclear spin-conserving transitions and then read

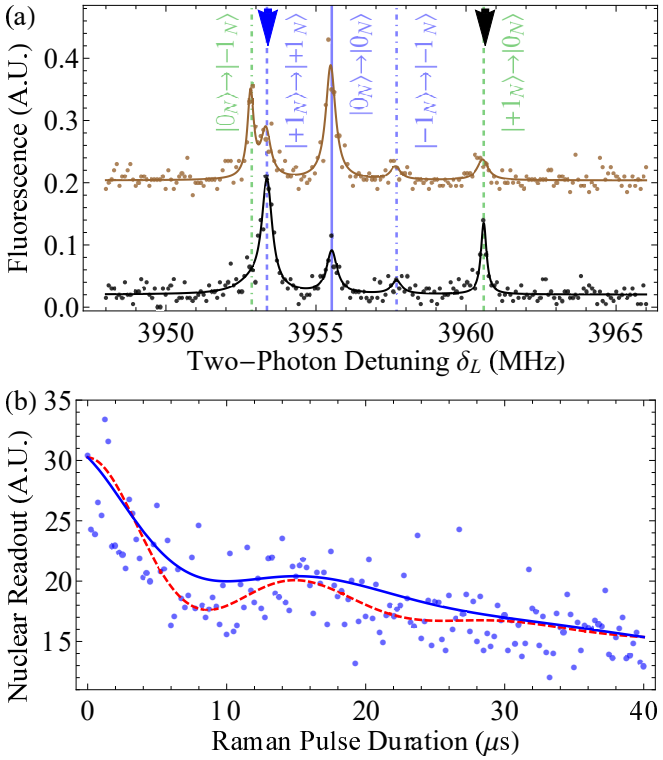

FIG. 4. Optical driving of the nuclear spin. (a) Spectroscopy of the Raman transition, conducted after a 40 μs pulse applied on the $|+1_N\rangle \rightarrow |0_N\rangle$ transition (brown, offset vertically for clarity) and after an equivalent wait time (black). (b) The $|+1_N\rangle$ population measured as a function of the duration of the $|+1_N\rangle \rightarrow |0_N\rangle$ Raman pulse, applied at the frequency indicated by the black arrow in (a). The blue plot is a maximum *a posteriori* fit to the data, and the red dashed plot is the result of a simulation of the Raman dynamics, as described in the Supplemental Materials [29].

out the electronic spin population optically. Because the optical transition we use to read out the $|+1\rangle$ population also pumps efficiently to $|0\rangle$, this nuclear readout process can be repeated many times in order to increase the information acquired during each run. The experiment can be performed in two manners, either by applying the readout π pulse on the $|+1_N\rangle \rightarrow |+1_N\rangle$ transition [blue arrow in Fig. 4(a)] to read out a signal proportional to the $|+1_N\rangle$ population [data in Fig. 4(b)], or analogously by measuring the $|0_N\rangle$ population (data in Supplemental Materials [29]). We note that, with optimization of the optical transitions that are used to read out and pump the electronic spin, this technique could potentially enable all-optical single-shot readout of the nuclear spin.

The results of this measurement are shown in Fig. 4(b). While the dominant feature is incoherent population transfer from $|+1_N\rangle$ to $|0_N\rangle$, Bayesian statistical analysis strongly suggests the presence of coherent oscillations [29]. Bayesian model comparison on the nuclear population data in Figs. 4(b) between the decaying oscillation model and multiple models of exponential decay favors the oscillatory model, and Bayesian parameter estimation yields the blue fit shown in Fig. 4(b).

We also simulate the expected Raman dynamics for both the nuclear spin-conserving transition (red dashed plot in Fig. 3) and the electronic-nuclear flip-flop transition [red dashed plot in Fig. 4(b)], assuming that decoherence of the Rabi oscillations is due solely to off-resonant optical excitation [29]. To match the data, we treat the Raman laser power and slight misalignment of the magnetic field as free parameters that are common to both plots. We set the simulations' vertical offsets to match the initial values of the data fit in Fig. 4(b) or the mean of the grey reference measurement in Fig. 3, and we set their vertical scalings to match the final values of the respective data fits. As shown in Fig. 4(b), the estimated frequency of the simulated dynamics closely matches that of the fit to the model of coherent oscillation, as described in the previous paragraph. Thus, our observations indicate the onset of coherent nuclear dynamics. However, the coherent oscillations are suppressed by decoherence due to optical pumping at a rate that is comparable to the Raman Rabi frequency.

To understand these observations and to explore the options for improving the nuclear optical control, we present a detailed theoretical analysis of this coupled electron-nuclear system [29]. While in general one can increase the Raman detuning Δ in order to suppress the incoherent optical pumping rate Γ relative to the Raman Rabi frequency $\tilde{\Omega}$, this approach is limited by destructive interference between the Raman transitions driven via $|E_1\rangle$ and $|E_y\rangle$ states, as we calculate explicitly in the Supplemental Materials [29]. Ultimately, the ratio $\tilde{\Omega}/\Gamma$ is determined by the strength of the interaction that mediates that specific Raman transition relative to the total decay rate out of the intermediate state. Therefore, while the coherence of the nuclear-spin conserving transitions may be improved by applying a small magnetic field transverse to the N-V axis to couple $|E_1\rangle$ and $|E_y\rangle$ via the Zeeman interaction, the coherence of the electronic-nuclear flip-flop transitions is limited by the fact that the transverse hyperfine coupling rate λ is comparable to the radiative decay rate γ out of the ^3E states ($\lambda/\gamma \approx 2$).

While this consideration limits the applicability of our technique, as implemented in the NV center, for performing high-fidelity quantum gates between electronic and nuclear spins, this limitation elucidates the properties of a quantum system that ultimately bound the technique's fidelity.

In conclusion, we have experimentally demonstrated control of a single nuclear spin state via coherent optical excitation. These proof-of-concept experiments can be extended along several promising directions. Better control of the transverse magnetic field would enable a precise measurement of the transverse hyperfine coupling strength in the excited state and a more detailed inves-

tigation of the ESLAC-based nuclear polarization mechanisms. Furthermore, similar techniques could be readily applied to other solid-state defects, such as silicon-vacancy centers, in which all-optical coherent manipulation of the SiV center's electronic spin has already been demonstrated [34, 35], or the divacancy defect center in 3C-SiC, which has a similar excited state structure and radiative decay rate but a hyperfine coupling rate of approximately 50 MHz with a proximal ^{13}C nucleus [36]. This optical manipulation technique could be particularly useful for densely spaced arrays of color centers integrated into nanophotonic devices [21], where it would enable the proximal nuclear spins to serve as the memory ancilla that are crucial for building quantum networks.

The authors would like to thank S. Singh and S. Choi for stimulating discussions, and Jamelle Watson-Daniels and Soumya Ghosh for their contribution to the development of the software used for the Bayesian analysis of the nuclear spin data. This work was supported by NSF, CUA, the DARPA QUEST program, AFOSR MURI, ARC, Element Six, and the Packard Foundation. This material is based upon work supported by the National Science Foundation Graduate Research Fellowship under Grant No. DGE1745303.

* mgoldman@post.harvard.edu

[1] P. Neumann, J. Beck, M. Steiner, F. Rempp, H. Fedder, P. R. Hemmer, J. Wrachtrup, and F. Jelezko, Science **329**, 542 (2010).
[2] P. C. Maurer, G. Kucsko, C. Latta, L. Jiang, N. Y. Yao, S. D. Bennett, F. Pastawski, D. Hunger, N. Chisholm, M. Markham, D. J. Twitchen, J. I. Cirac, and M. D. Lukin, Science **336**, 1283 (2012).
[3] G. D. Fuchs, G. Burkard, P. V. Klimov, and D. D. Awschalom, Nat. Phys. **7**, 789 (2011).
[4] M. V. Gurudev Dutt, L. Childress, L. Jiang, E. Togan, J. Maze, F. Jelezko, A. S. Zibrov, P. R. Hemmer, and M. D. Lukin, Science **316**, 1312 (2007).
[5] T. H. Taminiau, J. Cramer, T. van der Sar, V. V. Dobrovitski, and R. Hanson, Nat. Nanotechnol. **9**, 171 (2014).
[6] A. Reiserer, N. Kalb, M. S. Blok, K. J. M. van Bemmelen, T. H. Taminiau, R. Hanson, D. J. Twitchen, and M. Markham, Phys. Rev. X **6**, 021040 (2016).
[7] I. Lovchinsky, A. O. Sushkov, E. Urbach, N. P. de Leon, S. Choi, K. De Greve, R. Evans, R. Gertner, E. Bersin, C. Müller, L. McGuinness, F. Jelezko, R. L. Walsworth, H. Park, and M. D. Lukin, Science **351**, 836 (2016).
[8] G. Waldherr, Y. Wang, S. Zaiser, M. Jamali, T. Schulte-Herbrüggen, H. Abe, T. Ohshima, J. Isoya, J. F. Du, P. Neumann, and J. Wrachtrup, Nature (London) **506**, 204 (2014).
[9] J. Cramer, N. Kalb, M. A. Rol, B. Hensen, M. S. Blok, M. Markham, D. J. Twitchen, R. Hanson, and T. H. Taminiau, Nat. Commun. **7**, 11526 (2016).
[10] M. Hirose and P. Cappellaro, Nature (London) **532**, 77 (2016).
[11] B. B. Buckley, G. D. Fuchs, L. C. Bassett, and D. D. Awschalom, Science **330**, 1212 (2010).
[12] C. G. Yale, B. B. Buckley, D. J. Christle, G. Burkard, F. J. Heremans, L. C. Bassett, and D. D. Awschalom, Proc. Natl. Acad. Sci. U.S.A. **110**, 7595 (2013).
[13] Y. Chu, M. Markham, D. J. Twitchen, and M. D. Lukin, Phys. Rev. A **91**, 021801(R) (2015).
[14] C. G. Yale, F. J. Heremans, B. B. Zhou, A. Auer, G. Burkard, and D. D. Awschalom, Nat. Photon. **10**, 184 (2016).
[15] Y. Sekiguchi, N. Niikura, R. Kuroiwa, H. Kano, and H. Kosaka, Nat. Photon. **11**, 309 (2017).
[16] B. B. Zhou, P. C. Jerger, V. O. Shkolnikov, F. J. Heremans, G. Burkard, and D. D. Awschalom, Phys. Rev. Lett. **119**, 140503 (2017).
[17] E. Togan, Y. Chu, A. Imamoglu, and M. D. Lukin, Nature (London) **478**, 497 (2011).
[18] D. A. Golter, K. N. Dinyari, and H. Wang, Phys. Rev. A **87**, 035801 (2013).
[19] D. A. Golter and H. Wang, Phys. Rev. Lett. **112**, 116403 (2014).
[20] W. Pfaff, T. H. Taminiau, L. Robledo, H. Bernien, M. Markham, D. J. Twitchen, and R. Hanson, Nat. Phys. **9**, 29 (2012).
[21] R. E. Evans, M. K. Bhaskar, D. D. Sukachev, C. T. Nguyen, A. Sipahigil, M. J. Burek, B. Machielse, G. H. Zhang, A. S. Zibrov, E. Bielejec, H. Park, M. Lončar, and M. D. Lukin, Science **362**, 662 (2018).
[22] The hyperfine coupling can also, with the application of a suitable magnetic field, significantly enhance the nuclear gyromagnetic ratio through hybridization of the electronic and nuclear spins [3, 23–25]. This technique has enabled rapid RF-based manipulation of the nuclear spin but also increases its decoherence rate [3, 25].
[23] B. Smeltzer, J. McIntyre, and L. Childress, Phys. Rev. A **80**, 050302(R) (2009).
[24] M. Chen, M. Hirose, and P. Cappellaro, Phys. Rev. B **92**, 020101(R) (2015).
[25] S. Sangtawesin, C. A. McLellan, B. A. Myers, A. C. Bleszynski Jayich, D. D. Awschalom, and J. R. Petta, New J. Phys. **18**, 083016 (2016).
[26] V. Jacques, P. Neumann, J. Beck, M. Markham, D. Twitchen, J. Meijer, F. Kaiser, G. Balasubramanian, F. Jelezko, and J. Wrachtrup, Phys. Rev. Lett. **102**, 057403 (2009).
[27] M. Steiner, P. Neumann, J. Beck, F. Jelezko, and J. Wrachtrup, Phys. Rev. B **81**, 035205 (2010).
[28] C. Santori, P. Tamarat, P. Neumann, J. Wrachtrup, D. Fattal, R. G. Beausoleil, J. Rabeau, P. Olivero, A. D. Greentree, S. Prawer, F. Jelezko, and P. Hemmer, Phys. Rev. Lett. **97**, 247401 (2006).
[29] See Supplemental Material at [URL will be inserted by publisher], which includes Refs. [37–57], for detailed discussions of experimental methods and data analysis techniques.
[30] M. W. Doherty, N. B. Manson, P. Delaney, and L. C. L. Hollenberg, New J. Phys. **13**, 025019 (2011).
[31] G. D. Fuchs, V. V. Dobrovitski, R. Hanson, A. Batra, C. D. Weis, T. Schenkel, and D. D. Awschalom, Phys. Rev. Lett. **101**, 117601 (2008).
[32] M. L. Goldman, A. Sipahigil, M. W. Doherty, N. Y. Yao, S. D. Bennett, M. Markham, D. J. Twitchen, N. B. Manson, A. Kubanek, and M. D. Lukin, Phys. Rev. Lett. **114**, 145502 (2015).

[33] M. W. Doherty, F. Dolde, H. Fedder, F. Jelezko, J. Wrachtrup, N. B. Manson, and L. C. L. Hollenberg, Phys. Rev. B **85**, 205203 (2012).

[34] L. J. Rogers, K. D. Jahnke, M. H. Metsch, A. Sipahigil, J. M. Binder, T. Teraji, H. Sumiya, J. Isoya, M. D. Lukin, P. Hemmer, and F. Jelezko, Phys. Rev. Lett. **113**, 263602 (2014).

[35] B. Pingault, J. N. Becker, C. H. H. Schulte, C. Arend, C. Hepp, T. Godde, A. I. Tartakovskii, M. Markham, C. Becher, and M. Atatüre, Phys. Rev. Lett. **113**, 263601 (2014).

[36] D. J. Christle, P. V. Klimov, C. F. de las Casas, K. Szász, V. Ivády, V. Jokubavicius, J. Ul Hassan, M. Syväjärvi, W. F. Koehl, T. Ohshima, N. T. Son, E. Janzén, Á. Gali, and D. D. Awschalom, Phys. Rev. X **7**, 021046 (2017).

[37] L. C. Bassett, F. J. Heremans, C. G. Yale, B. B. Buckley, and D. D. Awschalom, Phys. Rev. Lett. **107**, 266403 (2011).

[38] L. Robledo, H. Bernien, I. van Weperen, and R. Hanson, Phys. Rev. Lett. **105**, 177403 (2010).

[39] F. Poggiali, P. Cappellaro, and N. Fabbri, Phys. Rev. B **95**, 195308 (2017).

[40] V. Ivády, K. Szász, A. L. Falk, P. V. Klimov, D. J. Christle, E. Janzén, I. A. Abrikosov, D. D. Awschalom, and A. Gali, Phys. Rev. B **92**, 115206 (2015).

[41] S. Nah, Mater. Res. Express **3**, 075008 (2016).

[42] L. J. Rogers, R. L. McMurtrie, M. J. Sellars, and N. B. Manson, New J. Phys. **11**, 063007 (2009).

[43] M. L. Goldman, M. W. Doherty, A. Sipahigil, N. Y. Yao, S. D. Bennett, N. B. Manson, A. Kubanek, and M. D. Lukin, Phys. Rev. B **91**, 165201 (2015).

[44] J. R. Maze, A. Gali, E. Togan, Y. Chu, A. Trifonov, E. Kaxiras, and M. D. Lukin, New J. Phys. **13**, 025025 (2011).

[45] L. C. Bassett, F. J. Heremans, D. J. Christle, C. G. Yale, G. Burkard, B. B. Buckley, and D. D. Awschalom, Science **345**, 1333 (2014).

[46] J. H. N. Loubser and J. A. van Wyk, Rep. Prog. Phys. **41**, 1201 (1978).

[47] X.-F. He, N. B. Manson, and P. T. H. Fisk, Phys. Rev. B **47**, 8809 (1993).

[48] S. Felton, A. M. Edmonds, M. E. Newton, P. M. Martineau, D. Fisher, D. J. Twitchen, and J. M. Baker, Phys. Rev. B **79**, 075203 (2009).

[49] N. R. S. Reddy, N. B. Manson, and E. R. Krausz, J. Lumin. **38**, 46 (1987).

[50] A. Gali, Phys. Rev. B **80**, 241204(R) (2009).

[51] M. W. Doherty, N. B. Manson, P. Delaney, F. Jelezko, J. Wrachtrup, and L. C. L. Hollenberg, Phys. Rep. **528**, 1 (2013).

[52] R. Ozeri, C. Langer, J. D. Jost, B. DeMarco, A. Ben-Kish, B. R. Blakestad, J. Britton, J. Chiaverini, W. M. Itano, D. B. Hume, D. Leibfried, T. Rosenband, P. O. Schmidt, and D. J. Wineland, Phys. Rev. Lett. **95**, 030403 (2005).

[53] K.-M. C. Fu, C. Santori, P. E. Barclay, L. J. Rogers, N. B. Manson, and R. G. Beausoleil, Phys. Rev. Lett. **103**, 256404 (2009).

[54] L. Robledo, H. Bernien, T. van der Sar, and R. Hanson, New J. Phys. **13**, 025013 (2011).

[55] G. Thiering and A. Gali, Phys. Rev. B **96**, 081115(R) (2017).

[56] S.E. Bialkowski, Anal. Chem. **61**, 2479-2483 (1989).

[57] D. Foreman-Mackey, D.W. Hogg, D. Lang, and J. Goodman, PASP **125**, 306–312 (2013).